Wideband and High Cross-Polarization Discrimination 45° Linearly Polarized Slot Array Antenna Without Cavity-Backed Layer

Zhou, Haijiao; Lu, Yunlong; You, Qingchun; Wang, Yi; Huang, Jifu

DOI:
10.1109/LAWP.2022.3187952

Wideband and High Cross-Polarization Discrimination 45° Linearly Polarized Slot Array Antenna Without Cavity-Backed Layer

Haijiao Zhou, Yunlong Lu, *Member, IEEE*, Qingchun You, Yi Wang, *Senior Member, IEEE*, and Jifu Huang

***Abstract*— This letter presents a wideband and high cross-polarization discrimination (XPD) 8×8-slot full corporate-feed 45° linearly polarized slot array antenna. A new vertical 1-to-4 power divider consisting of one H-plane T-junction and two E-plane T-junctions is employed to replace the 1-to-4 cavity-backed power divider in the conventional designs, which balances the amplitude and phase distributions among the output ports. By further bending the output ports of the 1-to-4 power dividers upward 90° along the diagonal plane, the TE_{10} mode in the signal path is smoothly shifted along the intended E- and H-planes and directly excites the 45° tilted radiation slots. Combined these features, the grating lobe suppression and XPD improvement over a wide frequency band can be achieved without introducing additional metal structures. For demonstration, a prototype covering 24-33 GHz is implemented. The experimental results are in good agreement with the simulation ones, which verifies the design concept.**

***Keywords*— 45° linearly polarized antenna, slot array antenna, high cross-polarization discrimination (XPD), wideband, low sidelobe levels (SLLs).**

I. Introduction

It is well known that the 45° linearly polarized antenna can achieve the low sidelobe level (SLL) characteristics in E- and H-planes [1]-[5]. The hollow-waveguide (HW) based 45° linearly polarized antennas are widely used in long-distance point-to-point wireless communication systems due to their high gain, high efficiency, and low SLLs [6], [7]. Bandwidth [8]-[11] and cross-polarization discrimination (XPD) [12]-[14] are two other key metrics for the 45° linearly polarized antennas, which help to improve the overall performance of point-to-point communication systems.

A common way to design a 45° linearly polarized antenna is to rotate the radiating slots by 45° [15]-[17]. To avoid grating lobes, the period between adjacent radiating elements is usually smaller than one free-space wavelength corresponding to the highest operating frequency in the bandwidth [18]-[22]. In such confined space, it is difficult to implement a full corporate-feed network that excites the radiating slots in a one-to-one correspondence. The conventional solution is to introduce an additional 1-to-4 cavity-backed power divider layer to simplify the layout of the feed network layer. However, the asymmetric structure in which the cavity-backed power divider excites the tilted radiation slots results in unbalanced excitation between the adjacent radiating slots (generating grating lobes). Combined further with the coupling of higher-order modes in the backed cavity into the tilted radiating slots, the XPD degrades significantly [23].

Some works have been reported to solve these drawbacks. In [23] and [24], an excitation slot layer is inserted between the 1-to-4 cavity-backed layer and the radiating layer to balance the amplitude and phase distributions. Meanwhile, the cross-polarization pattern is further improved by thickening the radiating slots or adding an extra narrow-slot pair layer on top of the radiating slot layer. But, this leads to an increase in the number of metal layers. It exacerbates the antenna complexity and the risk of electromagnetic leakage when conventional manufacturing processes (e.g., milling) are used instead of the process of diffusion bonding mentioned in the above works. The work [25] proposes another approach. The XPD and grating lobe suppression are optimized by loading triangular metal blocks in the 1-to-4 cavity-backed layer. But the fractional bandwidth (FBW) is limited to only 18.8% (26.5 -32 GHz). Although adding an additional 1-to-2 cavity-backed layer above the 1-to-4 cavity-backed layer can further expand the bandwidth (up to ~ 26.4%), it inevitably increases the number of metal layers [26]. How to achieve wideband and high XPD in HW-based 45° linearly polarized antennas without increasing metal layers remains a challenge.

This letter aims to tackle this challenge. A new vertical 1-to-4 power divider layer is used to replace the 1-to-4 cavity-backed layer in the previous works. It has two features: (i) equal and in-phase responses over a wide frequency band are obtained among the asymmetric output ports; (ii) only the fundamental mode (TE_{10}) propagates in the signal path exciting the tilted radiation slots. These properties completely overcome the disadvantages caused by the 1-to-4 cavity-backed layer, thereby facilitating the realization of a wideband high XPD 45° linearly polarized array antenna with reduced metal layers.

This work was supported partly by National Natural Science Foundation of China under Projects 62171242, U1809203, 61801252 and 61631012, in part by Zhejiang Provincial Natural Science Foundation of China under Project LY21F010002, and Ningbo Natural Science Foundation under Project 202003N4108. (*Corresponding author: Yunlong Lu; Jifu Huang.*)

H. Zhou, Y. Lu, and J. Huang are with the Faculty of Electrical Engineering and Computer Science, Ningbo University, Ningbo, Zhejiang, 315211, China (e-mail: luyunlong@nbu.edu.cn).

Q. You, and Y. Wang is with School of Engineering, University of Birmingham, B15 2TT, United Kingdom (e-mail: y.wang.1@bham.ac.uk).

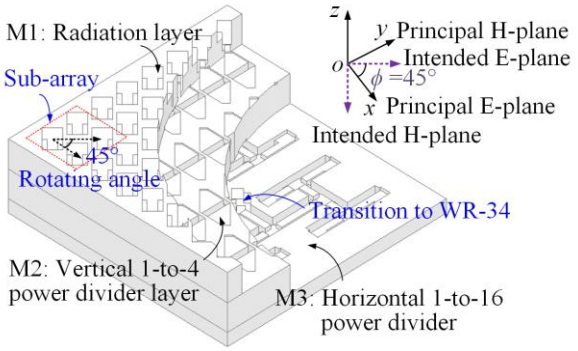

Fig. 1. Antenna configuration.

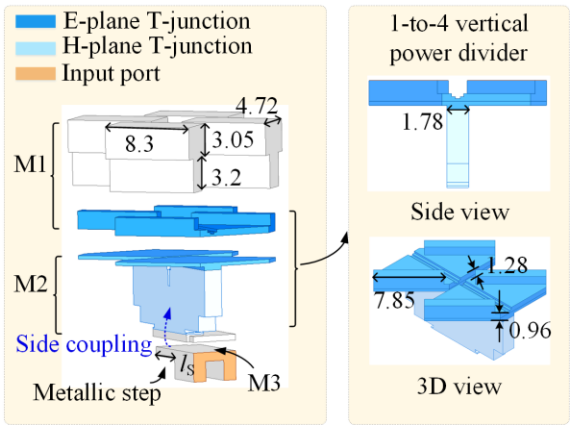

Fig. 2. Air model of the sub-array. All dimensions are given in millimeters.

II. Antenna Analysis and Design

A. Antenna configuration

Fig. 1 shows the configuration of the proposed 8 × 8-element 45° linearly polarized slot array antenna. It consists of the radiating part and the feeding part. The radiating part is the 45° tilted radiation slots in M1, while the feeding part contains the horizontal 1-to-16 power divider in M3 and the vertical 1-to-4 power dividers in M2. To reduce the number of metal layers, partial output structure of the vertical 1-to-4 power divider is incorporated into M1 (see clearly in Fig. 2). The new vertical 1-to-4 power divider composed of one H-plane T-junction and two E-plane T-junctions is used to replace the conventional 1-to-4 cavity-backed power divider, thereby overcoming the constraints brought by it (as discussed in introduction). In addition, the outputs of the vertical 1-to-4 power divider are directly rotated by 45° to support the radiating part. The signal from the output ports of the horizontal 1-to-16 power divider enters into the vertical 1-to-4 power divider layer and subsequently excites the radiation slots. The definition of the intended E- (ϕ = 45°) and H- (ϕ = 135°) planes and the principal E- (ϕ = 0°) and H- (ϕ = 90°) planes are also shown in Fig. 1. The concerned frequency band in this design is 24-33 GHz for 5G millimeter wave applications. All the simulation results are obtained by using Ansys HFSS.

B. Sub-array

The structure of the 2×2-slot sub-array together with the optimized dimensions is shown as Fig. 2. The space between adjacent radiation slots is set to 8 mm (0.88 λ_{min}, λ_{min} is the free-space wavelength corresponding to the highest operating frequency in the concerned frequency band), so as to avoid the generation of grating lobes. The two-step flared radiation slots are used to improve the impedance matching bandwidth between the radiation slot and the free space.

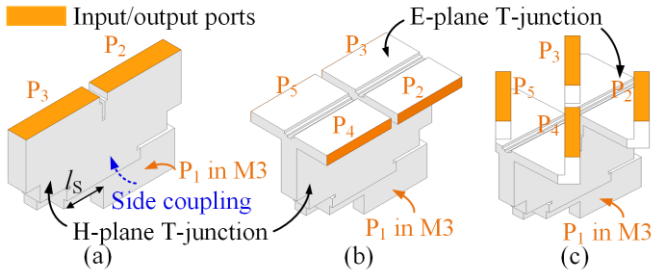

Fig. 3. Evolution of the vertical 1-to-4 power divider (air model). (a) Starting step with H-plane T-junction; (b) preliminary formation of the vertical 1-to-4 power divider; (c) desired vertical 1-to-4 power divider with bent outputs.

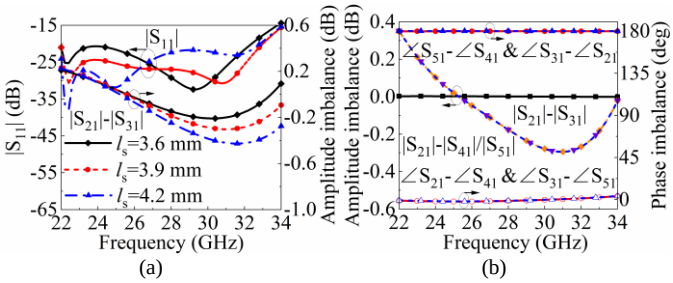

Fig. 4. Simulated results. (a) $|S_{11}|$ and amplitude imbalance between the output ports of the H-plane T-junction (Fig. 3(a)) with different values of l_S; (b) amplitude and phase responses of the vertical 1-to-4 power divider in Fig. 3(b).

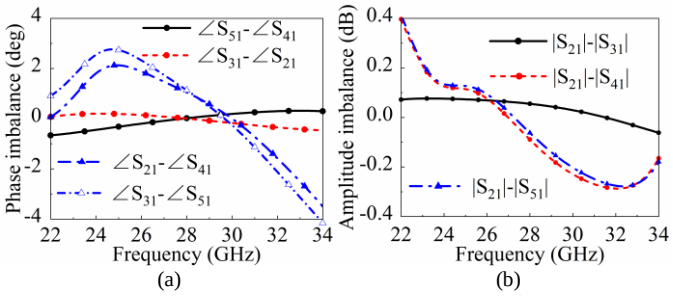

Fig. 5. Simulated (a) phase and (b) amplitude imbalances of the 1-to-4 power divider with 90° bent output ports.

A key part of the sub-array is the vertical 1-to-4 power divider that replaces the 1-to-4 cavity-backed power divider in the conventional designs. It is based on one H-plane T-junction and two E-plane T-junctions, and the design evolution is shown in Fig. 3. It starts with an H-plane T-junction in Fig. 3(a). The signal from each output port (P_1) of the power divider in M3 is side-coupled into the H-plane T-junction. To reduce the amplitude imbalance between the output ports of the H-plane T-junction caused by this side coupling structure, the metallic step (see in Fig. 2) is utilized in each single-ridge waveguide output branch of the 1-to-16 power divider. By adjusting the length of the metallic step (l_S), the amplitude imbalance can be optimized. Fig. 4(a) shows the corresponding simulated results. When l_S = 3.9 mm, the amplitude imbalance is controlled within the acceptable range (about 0.3 dB) and the $|S_{11}|$ is kept below -20 dB over the frequency range of 24-33 GHz.

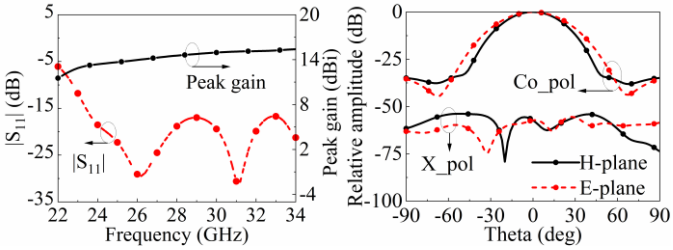

Fig. 6. Simulated performance of sub-array. (a) $|S_{11}|$ and peak gain; (b) radiation patterns at 28.5 GHz.

Following, two E-plane T-junctions are cascaded with the H-plane T-junction to construct a vertical 1-to-4 power divider, as shown in Fig. 3(b). Fig. 4(b) plots the simulated amplitude and phase responses. Slight amplitude difference (still within 0.3 dB) is existed between the output ports 2(3) and 4(5), due to the amplitude imbalance between the output ports in the H-plane T-junction. Meanwhile, the out-of-phase response caused by the E-plane T-junctions is obtained between the ports 2(4) and 3(5). To support the 45° tilted radiation slots, all output ports of vertical 1-to-4 power divider are further bent upwards by 90° along the diagonal plane, as shown in Fig. 3(c). Benefit from the inherent out-of-phase property between bent ports 2(4) and 3(5), the aforementioned out-of-phase responses in Fig. 4(b) can be compensated. The simulated results in Fig. 5 verify this. It can be seen that all output ports are in-phase (0°±3.2°) now in the desired frequency range of 24-33 GHz, and the amplitude imbalance is still less than 0.3 dB at the same time.

Another key objective of this work is to suppress the cross-polarization patterns. Although some structures have been proposed to improve XPD in the previous works [25], [26], they only serve as optimizations and do not fundamentally solve this issue. In this design, the 90° upward bent output ports of the vertical 1-to-4 power divider have been rotated by 45° to directly excite the radiation slots. This means that only the TE_{10} mode propagates in the signal path and is smoothly shifted along the intended E- and H-planes. Combined with the wideband equal-amplitude in-phase response of the vertical 1-to-4 power divider, the XPD can be substantial improved. Fig. 6 shows the simulated performance of the 2×2-slot sub-array. The radiation patterns in the intended E- and H-planes are obtained at 28.5 GHz. The SLL is suppressed to below -30 dB and the XPD is optimized to exceed 50 dB. Over the desired frequency range, the reflection coefficient is less than -15 dB and the peak gain is higher than 14.1 dBi.

C. Horizontal 1-to-16 power divider

The whole proposed array antenna is built using 16 (4×4) such 2×2-slot sub-arrays. A 1-to-16 power divider in M3 is designed to support the sub-arrays. The layout of the power divider is shown in Fig. 7(a). It is based on multiple H-plane single-ridge waveguide T-junctions. It should be noted that partial single-ridge waveguide structure in each output branch is included in the sub-array (see Fig. 2) and is not shown here.

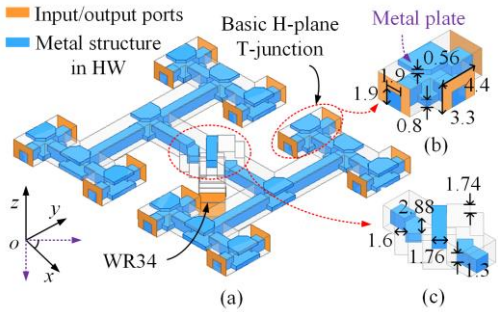

Fig. 7. Horizontal 1-to-16 feed network. (a) Layout of the whole feed network; (b) basic H-plane T-junction; (c) transition E-plane power divider. All dimensions are given in millimeters.

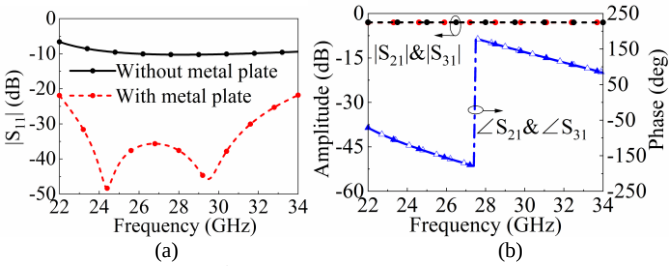

Fig. 8. Simulated results of the basic H-plane T-junction. (a) $|S_{11}|$; (b) amplitude and phase responses at the output ports.

The basic H-plane T-junction is shown in Fig. 7(b). An additional metal plate embedded in the upper wall of the single-ridge waveguide T-junction is employed to improve the impedance matching. With the optimized dimensions shown in Fig. 7(b), the comparison of reflection coefficients with and without the metal plate is plotted in Fig. 8(a). It is effectively improved over a wide frequency band by adding the metal plate. The amplitude and phase responses of the basic H-plane T-junction are also shown in Fig. 8(b). Good equal-amplitude and in-phase responses are obtained over the frequency range of 24 - 33 GHz. A standard waveguide input port (WR34) is located at the back center of the power divider. A transition E-plane power divider is utilized to match the input HW to the output single-ridge waveguide, as shown in Fig. 7(c). Besides, the standard waveguide input port is rotated to parallel with the radiation slots, so that for easy measurement. The design details of the transition power divider can be founded in author's previous work [25], which is not repeated here. Finally, the whole 1-to-16 power divider exhibits good amplitude and phase responses over the desired frequency range.

III. Experimental Results

As indicating in Fig. 1, the prototype is divided into three metal blocks (radiating part in M1, vertical 1-to-4 power divider in M2, and horizontal 1-to-16 power divider in M3) for fabrication using aluminum by milling with a tolerance of 20 μm. Screws are used to suppress the potential electromagnetic energy leakage and assemble the prototype. The photographs of the fabricated metal blocks, assembled antenna and test environment are shown in Fig. 9. The overall size of the fabricated antenna is 74×74×18.4 mm^3. The antenna profile height is comparable to previous works. The radiation performances are measured by a near-field test system in an anechoic chamber.

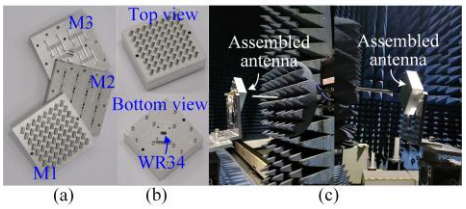

Fig. 9. Photos of (a) separated metal blocks, (b) assembled antenna and (c) test environment.

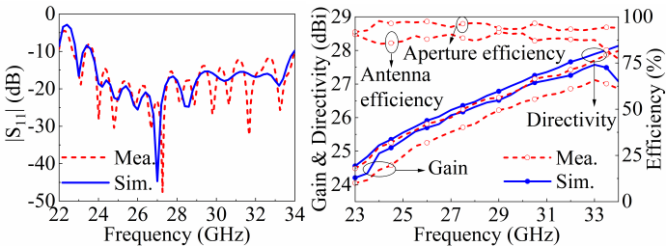

Fig. 10. Simulated and measured results. (a) $|S_{11}|$; (b) peak gain, directivity and antenna efficiency.

A. *Reflection Coefficient, Peak Gain and Efficiency*

The simulated and measured reflection coefficients are shown in Fig. 10(a). The measured result is carried out by using an Agilent E8361C network analyzer. They are in a good agreement. The impedance matching bandwidth of $|S_{11}|$<-10 dB is from 24 GHz to 33 GHz (FBW: 31.5%). Fig. 10(b) illustrates the simulated and measured peak gain, directivity and antenna efficiency. The measured peak gain varies from 24.4 dBi to 27.1 dBi over the frequency range of 24-33 GHz, which is about 0.2-0.5 dBi lower than the simulated result. The measured directivity is within the range of 25.1 – 27.7 dBi, while the simulated one varies between 25.2 dBi and 27.9 dBi. The slight difference is mainly attributed to the fabrication tolerance, assemble and measurement errors. Based on the measured peak gain and directivity, the calculated antenna total efficiency is better than 85.3% across the whole frequency band. Meanwhile, the measured antenna aperture efficiency is over 92.6%.

B. *Radiation Patterns*

Fig. 11 shows the simulated and measured radiation patterns in the intended E- and H-planes. The measured results are in a good agreement with the simulated ones. Compared with SLLs (about −13 dB) in the principal E- and H-planes, the measured SLLs in the intended E- and H-planes are suppressed to less than 25.9 dB over the desired frequency range. The cross-polarization patterns are also plotted in Fig. 11. The measured XPD is more than 45.8 dB in all planes, exhibiting good cross-polarization pattern suppression.

Table I compares this work with some other 45° linearly polarized antennas. All the works are based on HW (or air-filled gap waveguide). Both the work [25] and this design are implemented based on a three-layer metal structure, and other works have more metal layers. Thanks to the elimination of the 1-to-4 cavity-backed layer, the proposed antenna achieves the widest impedance bandwidth and highest XPD while maintaining comparable radiation performance, such as SLL, antenna efficiency, etc.

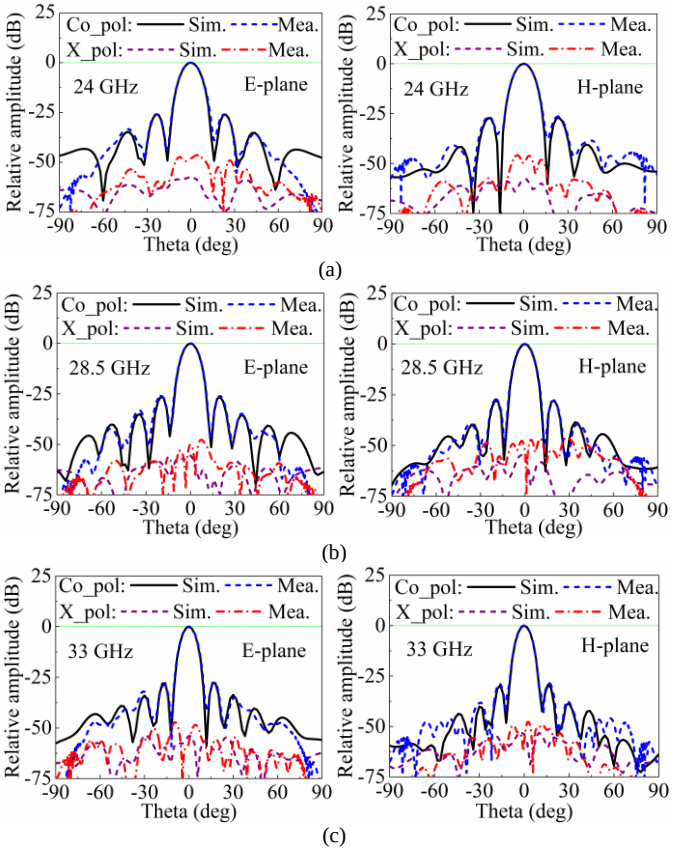

Fig. 11. Simulated and measured radiation patterns in the intended E-plane and H-plane at: (a) 24 GHz; (b) 28.5 GHz; (c) 33 GHz.

TABLE I
COMPARISON OF WAVEGUIDE ANTENNA ARRAYS

Ref.	Antenna type	f (GHz) /BW (%)	SLL (dB)	*Eff. (%)	*Gain (dBi)	XPD (dB)
[23]	HW+16×16 slots	61.5/9.6	-25.5	89.2	32.8	>31.5
[24]	HW+16×16 slots	78.5/20.4	-26.2	86.6	32.9	>30
[25]	HW+8×8 slots	29.25/18.8	-26.2	89.7	26.9	>31.3
[26]	GW#+8×8 slots	26.5/26.4	-25.8	85.8	26	>30.2
This work	HW+8×8 slots	28.5/31.5	-25.9	88.8	26.1	>45.8

#GW: gap waveguide. *They are obtained at the center frequency of the operating frequency band.

IV. CONCLUSION

A HW based wideband high-performance 45° linearly polarized slot array antenna has been proposed in this letter. The 1-to-4 cavity-backed layer in the conventional designs was replaced by a new vertical 1-to-4 power divider layer. This can substantially overcome the XPD degradation and the amplitude and phase imbalances between the adjacent radiation slots caused by the 1-to-4 cavity-backed layer without additional structures. A prototype of 8×8-slot array antenna with stable radiation bandwidth of 24-33 GHz was demonstrated. Experimental results validate the design concept. The features of wideband, high XPD, low SLL, high gain render this antenna a good candidate for millimeter-wave point-to-point communication systems.

REFERENCES

[1] D. Kim, W. Chung, C. Park, S. Lee, and S. Nam, "Design of a 45°-inclined SIW resonant series slot array antenna for Ka band," *IEEE Antennas Wireless Propag. Lett.*, vol. 10, pp. 318-321, 2011.

[2] Y. Quan, H. Wang, S. Tao, and J. Yang, "A double-layer multibeam antenna with 45° linear polarization based on gap waveguide Technology," *IEEE Trans. Antennas Propag.*, vol. 70, no. 1, pp. 56-66, Jan. 2022.

[3] D.-Y. Kim, W.-S. Chung, C.-H. Park, S.-J. Lee, and S. Nam, "A series slot array antenna for 45°-inclined linear polarization with SIW technology," *IEEE Trans. Antennas Propag.*, vol. 60, no. 4, pp. 1785-1795, Apr. 2012.

[4] J. Hirokawa, and M. Ando, "45° linearly polarized post wall waveguide-fed parallel plate slot arrays," *IEE Proc., Microw. Antennas Propag.*, vol. 147, pp. 515–519, Dec. 2000.

[5] Y. Hayashi, K. Sakakibara, M. Nanjo, S. Sugawa, N. Kikuma, and H. Hirayama, "Millimeter-wave microstrip comb-line antenna using reflection-canceling slit structure," *IEEE Trans. Antennas Propag.*, vol. 59, no. 2, pp. 398-406, Feb. 2011

[6] Y. You et al., "High-performance E-band continuous transverse stub array antenna with a 45° linear polarizer," *IEEE Antennas Wireless Propag. Lett.*, vol. 18, no. 10, pp. 2189–2193, Oct. 2019.

[7] Fixed Radio Systems, Characteristics and Requirements for Point-to-Point Equipment and Antennas, ETSI EN 302 217-4-2, v1. 5.1, Jan. 2010. [Online]. Available: https://www.etsi.org/index.php.

[8] A. Dastranj, and B. Abbasi-Arand, "High-performance 45° slant-polarized omnidirectional antenna for 2–66-GHz UWB applications," *IEEE Trans. Antennas Propag.*, vol. 64, no. 2, pp. 815-820, Feb. 2016.

[9] M.-B. Cai, Z.-H. Yan, F.-F. Fan, S.-Y. Yang, and X. Li, "Double-layer 45° linearly polarized wideband and highly efficient transmitarray antenna," *IEEE Open J. Antennas Propag.*, vol. 2, pp. 104-109, 2021.

[10] P. Fei, Y. Qi, and Y. Jiao, "Design of a wideband dual-element slot loop antenna array with adjustable back-reflector," *IEEE Antennas Wireless Propag. Lett.*, vol. 11, pp. 1014-1017, 2012.

[11] Y. Yu, W. Hong, Z. H. Jiang, and H. Zhang, "E-band low-profile, wideband 45° linearly polarized slot-loaded patch and its array for millimeter-wave communications," *IEEE Trans. Antennas Propag.*, vol. 66, no. 8, pp. 4364-4369, Aug. 2018.

[12] Y. Luo, Q. Chu, and D. Wen, "A plus/minus 45 degree dual-polarized base-station antenna with enhanced cross-polarization discrimination via addition of four parasitic elements placed in a square contour," *IEEE Trans. Antennas Propag.*, vol. 64, no. 4, pp. 1514-1519, April 2016.

[13] T. Yang, Z. Zhao, D. Yang and Z. Nie, "Low cross-polarization SIW slots array antenna with a compact feeding network," *IEEE Antennas Wireless Propag. Lett.*, vol. 20, no. 2, pp. 189-193, Feb. 2021.

[14] B. Li, Y. X. Z. Yin, W. Hu, Y. Ding, and Y. Zhao, "Wideband dual-polarized patch antenna with low cross polarization and high isolation," *IEEE Antennas Wireless Propag. Lett.*, vol. 11, no. 4, pp. 427-430, Apr. 2012.

[15] B. Liu et al., "A 45° linearly polarized slot array antenna with substrate integrated coaxial line technique," *IEEE Antennas Wireless Propag. Lett.*, vol. 17, no. 2, pp. 339-342, Feb. 2018.

[16] H. Zhou, W. Hong, L. Tian, and M. Jiang, "A balanced-fed 45° linearly polarized slot array antenna using SIW technology," *2015 9th European Conference on Antennas and Propagation (EuCAP)*, Lisbon, 2015, pp. 1–4.

[17] A. B. Guntupalli, and K. Wu, "45° linearly polarized high-gain antenna array for 60-GHz radio," *IEEE Antennas Wireless Propag. Lett.*, vol. 13, pp. 384-387, 2014.

[18] S. Shad, and H. Mehrpouyan, "60 GHz waveguide-fed cavity array antenna by multistepped slot sperture," *IEEE Antennas Wireless Propag. Lett.*, vol. 19, no. 3, pp. 438-442, Mar. 2020.

[19] H. Zhao et al., "E-band full corporate-feed 32 × 32 slot array antenna with simplified assembly," *IEEE Antennas Wireless Propag. Lett.*, vol. 20, no. 4, pp. 518-522, Apr. 2021.

[20] Y. Miura, J. Hirokawa, M. Ando, K. Igarashi, and G. Yoshida, "A circularly-polarized aperture array antenna with a corporate-feed hollow-waveguide circuit in the 60 GHz-band," *Proc. IEEE Int. Symp. Antennas Propag. (AP-S)*, pp. 3029-3032, Jul. 2011.

[21] M. Ferrando-Rocher, J. I. Herranz-Herruzo, A. Valero-Nogueira, and M. Baquero-Escudero, "Dual-band single-layer slot array antenna fed by K/Ka-band dual-mode resonators in gap waveguide technology," *IEEE Antennas Wireless Propag. Lett.*, vol. 20, no. 3, pp. 416-420, Mar. 2021.

[22] L. Qin, Y. Lu, Q. You, Y. Wang, J. Huang, and P. Gardner, "Millimeter-wave slotted waveguide array with unequal beamwidths and low sidelobe levels for vehicle radars and communications," IEEE Trans. Veh. Technol., vol. 67, no. 11, pp. 10574-10582, Nov. 2018.

[23] T. Tomura, Y. Miura, M. Zhang, J. Hirokaw, and M. Ando, "A 45° linearly polarized hollow-waveguide corporate-feed slot array antenna in the 60-GHz band," *IEEE Trans. Antennas Propag.*, vol. 60, no. 8, pp. 3640-3646, Aug. 2012.

[24] T. Tomura, J. Hirokawa, T. Hirano, and M. Ando, "A 45° linearly polarized hollow-waveguide 16×16-slot array antenna covering 71–86 GHz band," *IEEE Trans. Antennas Propag.*, vol. 62, no. 10, pp. 5061-5067, Oct. 2014.

[25] Y. You, Y. Lu, T. Skaik, Y. Wang, and J. Huang, "Millimeter-wave 45° linearly polarized corporate-fed slot array antenna with low profile and reduced complexity," *IEEE Trans. Antennas Propag.*, vol. 69, no. 9, pp. 6064-6069, Sep. 2021.

[26] L. Zhang et al., "Wideband 45° linearly polarized slot array antenna based on gap waveguide technology for 5G millimeter-wave applications," *IEEE Antennas Wireless Propag. Lett.*, vol. 20, no. 7, pp. 1259-1263, Jul. 2021.